Effects of Aromatic Substitutions on the Photoreactions in $Mg^{\bullet+}(C_6H_nF_2X_{4-n})$ (X = F, CH_3) Complexes: Formation and Decomposition of Benzyne Radical Cations

Haichuan Liu, Xinhao Zhang, Changsheng Wang,† Wenyue Guo,‡ Yundong Wu,* and Shihe Yang*

Department of Chemistry, The Hong Kong University of Science and Technology, Clear Water Bay, Kowloon, Hong Kong

Received: November 19, 2003; In Final Form: February 7, 2004

Photoinduced reactions have been systematically studied on mass-selected complexes of $Mg^{\bullet+}$ with tri- and tetrasubstituted benzene by F and/or CH_3. The complexes fall into two groups. The Group I complexes involve bidentate coordination of the *o*-F atoms to $Mg^{\bullet+}$, whereas the Group II complexes feature the linkage of $Mg^{\bullet+}$ to only one of the F atoms. The *o*-benzyne radical cations were found to be the predominant photolysis products from the Group I complexes, but the yields of the benzyne radical cation products were low for Group II. For each group of complexes, different substituents, including CH_3 (medium σ-electron donor) and F (strong σ-electron acceptor and weak π-electron donor), affect the branching ratios significantly. For example, they result in different decomposition thresholds of the *o*-benzyne radical cations. Through the studies of aromatic substitution, the pathways for the formation and decomposition of *o*-benzyne radical cations have been brought to light. With the help of quantum mechanics calculations, the observed substitutent effects on the photoformation and decomposition of the *o*-benzyne radical cations are explained mainly from the energy point of view. We found that although *o*-benzyne radical cations are formed by the direct abstraction of the F atoms, the formation of *m*-benzyne radical cations is stepwise, involving a π-$^{+}$MgF intermediate.

Introduction

There has been considerable interest in biradical benzynes (*o*-, *m*-, and *p*-benzyne) due to the fundamental and practical importance of these species.[1] For example, *o*-benzyne is a very reactive intermediate in various organic chemical reactions. Recently, it has been discovered that *p*-benzyne derivatives formed by Bergman cyclization reactions are involved in the DNA-cleaving activity of calicheamicin and related antitumor agents and antibiotics.[2−4] Using matrix isolation technique, infrared spectra of *o*-, *m*-, and *p*-benzyne and their fluorine-substituted derivatives have been obtained,[5,6] from which the structural information was extracted with the help of theoretical calculations. Spectroscopy of these species have also been studied in the gas phase to understand their electronic structures and dynamics.[5,7,8] Extensive computations were carried out to optimize the structures and to determine the physical parameters of benzynes using different methods, including CCSD(T), DFT, SCF, CI, or MP2 with different basis sets.[1,9] Substituted benzynes have also been studied. An important issue has been the tuning of the singlet−triplet energy gap (ΔE_{ST}) by substitution, which dictates the reactivity of the benzyne species.[7,10,11]

Negatively charged benzynes were recently synthesized in a flowing afterglow triple quadrupole instrument.[12] The singlet−triplet energy gaps have been obtained from their electronic spectra. The reactivity of the isomeric benzyne anions has also been studied with various reagents.[12,13] Freiser et al. produced an organometallic distonic cation $^{+}FeC_6H_4^{\bullet}$ through the reaction of laser-desorbed Fe^{+} with 1,4-diiodobenzene,[14a] and its chemistry was found to be unique in comparison to its even-electron counterpart Fe(*o*-benzyne)$^{\bullet+}$.[14b−e] Complexes of Ln^{+}−benzyne were also synthesized by reactions of laser-ablated Ln^{+} with cyclic hydrocarbons and identified by time-of-flight mass spectrometry.[15]

The information on benzyne radical cations has come mainly from photoionization and photoelectron spectroscopy of the neutral benzynes generated by high-temperature pyrolysis.[7,16−18] Zhang and Chen showed that the ground state of *o*-$C_6H_4^{\bullet+}$ is from the ionization of the π-electron of the corresponding neutral benzyne and that the ionization of the σ-electron is 0.72 eV higher in energy.[7] Very recently, our studies on photodissociation of mass-selected complexes of $Mg^{\bullet+}$ with organic halide molecules led to the finding of a convenient method for the production of benzyne radical cations.[19] Specifically, the *o*-, *m*-, and *p*-benzyne radical cations ($C_6H_4^{\bullet+}$) can be efficiently formed by the photodissociation of precursor complexes $Mg^{\bullet+}$(*o*-, *m*-, *p*-$C_6H_4F_2$). The photoreactions seem to occur through an electron transfer from the photoexcited $(Mg^{\bullet+})^{*}$, with the successive abstraction of the two negatively charged F^{-} species by Mg^{2+}, forming the benzyne radical cations and a stable neutral molecule MgF_2. Another interesting observation is that all the isomeric benzyne radical cations can undergo further decomposition to form $C_4H_2^{\bullet+}$ and C_2H_2. In particular, we have examined the metastable decay of *o*-$C_6H_4^{\bullet+}$ to $C_4H_2^{\bullet+}$ and C_2H_2, and bracketed the threshold of the ring-opening process to ∼1.7−2.4 eV. This suggests that most of the available energy from the primary photoreaction is deposited on the benzyne radical cation probably through the excited electron transfer.

In the work presented here, we have studied in some detail the effect of the aromatic substitutions by F and CH_3 on the photolysis of the complexes of $Mg^{\bullet+}$ and substituted benzenes,

* Corresponding authors. E-mail: chydwu@ust.hk (Y.W.); chsyang@ust.hk (S.Y.).

† Permanent address: Department of Chemistry, Liaoning Normal University, Dalian, People's Republic of China.

‡ Permanent address: Applied Physics Department, University of Petroleum, China, Dongying, Shandong 257061, People's Republic of China.

10.1021/jp037535+ CCC: $27.50
Published on Web 03/19/2004

as well as on the subsequent decomposition of the benzyne radical cations. The goal is to gain a better understanding of the pathways, energetics, and dynamics of the remarkable photoinduced reactions in the well-defined metal−organic molecule complexes. The knowledge of the photochemistry will allow the control of the reaction pathways, hence the optimization of desired product yields.

Experiments and Computations

The cluster apparatus for the present experiments has been described elsewhere,[20] so only a brief description is given here. A rotating magnesium disk (∼1.65 cm in diameter) attached to a sample holder was mounted 15 mm downstream from the exit of a pulsed valve (General Valve). Driven by a step motor, the sample disk rotated on each laser pulse to expose fresh surfaces during the laser-ablation experiments. The pulsed valve was employed to generate beams of difluorotoluene, trifluorotoluene, trifluorobenzene, and tetrafluorobenzene by supersonic expansion of the vapor seeded in helium with a backing pressure of ∼10 psi through a 0.5 mm diameter orifice. The second harmonic (532 nm) of a Nd:YAG laser (∼40 mJ/pulse) was weakly focused on a ∼1 mm diameter spot of the magnesium disk for the generation of metal cations. The laser-produced species containing metal ions and atoms traversed perpendicularly to the supersonic jet stream 20 mm from the ablation sample target, forming a series of metal cations solvated by the substituted benzene molecules. The nascent complexes and clusters then traveled 14 cm down to the extraction region of the reflectron time-of-flight spectrometer (RTOFMS).

The cation−molecule complexes were accelerated vertically by a high-voltage pulse in a two-stage extractor. After extraction, the cluster cations were steered by a pair of horizontal plates and a pair of vertical deflection plates. All the cluster cations were reflected by the reflectron and finally detected by a dual-plate microchannel plate detector (MCP). For photodissociation experiments, a two-plate mass gate equipped with a high-voltage pulser was used to select desired cluster cations. The mass-selected cluster cations, once arrived at the turn-around region of the reflectron, were irradiated with a collimated beam of a dye laser for photolysis. The parent and nascent daughter cations were re-accelerated by the reflectron electric field and detected by the MCP detector. The dye laser was pumped by a XeCl excimer laser (Lambda-Physik LPX210i/LPD3002). The spectral region of 335−450 nm was covered by the fundamental outputs of the dye laser using *p*-terphenyl, DMQ, BBQ, Stilbene 1, and Coumarin 440. For the spectral region of 230−335 nm, the second harmonic outputs were employed using DCM, Kiton Red, Coumarin 540A, Coumarin 503, and Coumarin 480. The branching fraction of each fragment was obtained from the corresponding photodissociation difference mass spectrum at different wavelengths.

The parent complexes and relevant substituted benzyne radical cations have been studied theoretically by the density functional theory (DFT) method of B3LYP with the GAUSSIAN 98 package.[21] Although the B3LYP method might have problems dealing with the radical cation systems,[22] the computational results at the level of B3LYP/6-31+G** can be used as a guide for the interpretation of our data especially for the substituted benzyne radical cations of low symmetry.[22] The problem should be less severe for the present study because the substituted benzyne radical cations are only of low symmetry. Each structure was fully optimized with the B3LYP/6-31+G** level followed by vibrational frequency calculation. Zero-point energy (ZPE) corrections were made for all of the energy values

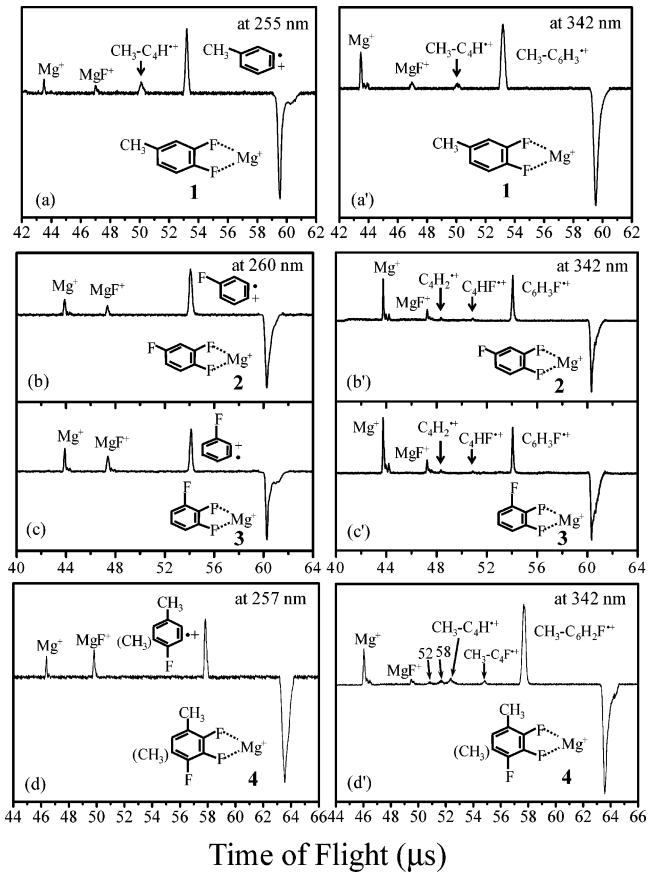

Figure 1. Photodissociation difference mass spectra of $Mg^{\bullet+}$(3,4-difluorotoluene), $Mg^{\bullet+}$(1,2,4-trifluorobenzene), $Mg^{\bullet+}$(1,2,3-trifluorobenzene), and $Mg^{\bullet+}$(2,3,4-trifluorotoluene) at short (250−260 nm) and long wavelengths (∼340 nm).

reported in this paper. The vertical excitation energies and the corresponding oscillator strengths of selected complexes were calculated with the CIS/6-31+G** method based on the B3LYP/6-31+G** geometries.

Results

A. Photodissociation Difference Mass Spectra. Photodissociation difference mass spectra of the complexes containing tri- and tetrasubstituted benzenes (**1**−**7**) are presented in Figures 1 and 2, respectively, at short and long laser wavelengths. The downward peaks in Figures 1 and 2 represent the depletion of the parent cations due to photolysis, while the upward peaks signify the corresponding formation of the daughter cations. Photodissociation of all these complexes produces mainly substituted benzyne radical cations, $Mg^{\bullet+}$, and MgF^+. The benzyne radical cations result from photoinduced MgF_2 elimination reactions, and MgF^+ is probably a side product of these processes. $Mg^{\bullet+}$ is an evaporative photofragment from the direct complex decomposition. The benzyne radical cations produced are believed to be of the ortho type because the common structural feature of these complexes is that they all contain neighboring F substitutions in the benzene ring.

At the short wavelengths of photolysis, the benzyne radical cations from all the complexes containing purely fluorinated benzenes or 2,3,4-trifluorotoluene (**2**−**7**) did not undergo further [4 + 2] dissociation. However, such dissociation products were observed at the longer wavelengths by two-photon excitation due to the increased laser fluence. Two-photon photolysis of tetra-F-substituted complexes even yielded a small amount of $MgF_2^{\bullet+}$, which may result from the increased ionization energy

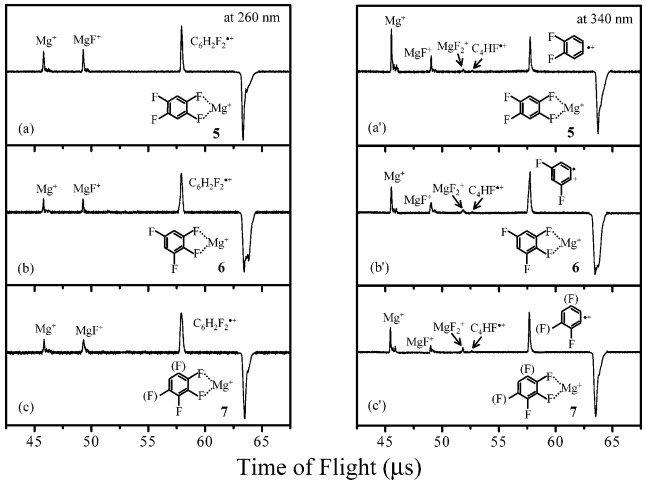

Figure 2. Photodissociation difference mass spectra of $Mg^{\bullet+}$(1,2,4,5-, 1,2,3,5-, and 1,2,3,4-tetrafluorobenzene) at 260 and 340 nm.

of the benzyne radical induced by F substitutions. For the complex of $Mg^{\bullet+}$(3,4-difluorotoluene) (**1**), on the other hand, dissociation from the benzyne radical cation to $CH_3-C_4H^{\bullet+}$ was observed at both the short and long wavelengths with a single photon. This suggests that the former is a much higher energy process than the latter due to the F substitution.

The photodissociation difference mass spectra of **4** (Figure 1d,d′) are quite similar to those of other complexes containing *o*-F-substituted benzenes except that two new photoproducts at $m/e = 52$ and 58 are observed at long wavelengths. These two photoproducts can be assigned to $CH_3CCCH^{\bullet+}$ and CH_3MgF^+ (or $CH_3C_2F^{\bullet+}$). It seems that the simultaneous presence of the CH_3 and F substituents on the *o*-benzyne radical cations opens more decomposition pathways that are very different from the typical [4 + 2] ring-opening channel.

Figure 3 shows photodissociation difference mass spectra of the complexes without neighboring fluorine substitutions on the benzene ring, namely $Mg^{\bullet+}$[2,4-$(CH_3)C_6H_3F_2$] (**8**), $Mg^{\bullet+}$[2,6-$(CH_3)C_6H_3F_2$] (**9**), and $Mg^{\bullet+}$(1,3,5-$C_6H_3F_3$) (**10**). Compared to the data in Figures 1 and 2, several features are noteworthy:

(1) Benzyne radical cations are still formed but with much reduced intensity. This is understandable because, in these complexes, $Mg^{\bullet+}$ is linked to only one F atom, whereas $Mg^{\bullet+}$ is coordinated with two neighboring fluorine atoms in **1**−**7**.

(2) A small amount of molecular ions, which result from direct charge transfer dissociation, is observed in most cases (see Figure 3).

(3) The yield of MgF^+ in the short wavelength region is significantly increased compared to that in the long wavelength region (especially for **9**), while $Mg^{\bullet+}$ is dominant in both wavelength regions. Overall, the reactive channels are dominated by photoinduced charge transfer, which leads to the molecular ions and other photoproducts.

B. Photodissociation Action Spectra. Shown in Figures 4−6 are action spectra and branching fraction curves of $Mg^{\bullet+}$-(trisubstituted benzene) (**1**−**3**), $Mg^{\bullet+}$(tetrasubstituted benzene) (**5**−**7**), and $Mg^{\bullet+}$(*m*-trisubstituted benzene) (**8**, **10**), respectively, in the wavelength range of ∼230−440 nm. In the action spectra, the solid lines indicate the atomic transition of $Mg^{\bullet+}$($3^2P \leftarrow 3^2S$) and the dashed lines denote the calculated absorption spectra using the CIS method. $Mg^{\bullet+}$(1,2,3,4-$C_6H_2F_4$) has two possible isomers: one is with $Mg^{\bullet+}$ coordination to the 1,2-F atoms and the other is with $Mg^{\bullet+}$ coordination to the 2,3-F atoms. In this case, the corresponding calculated absorption spectra are shown in dashed and dotted lines, respectively (Figure 5c). Overall,

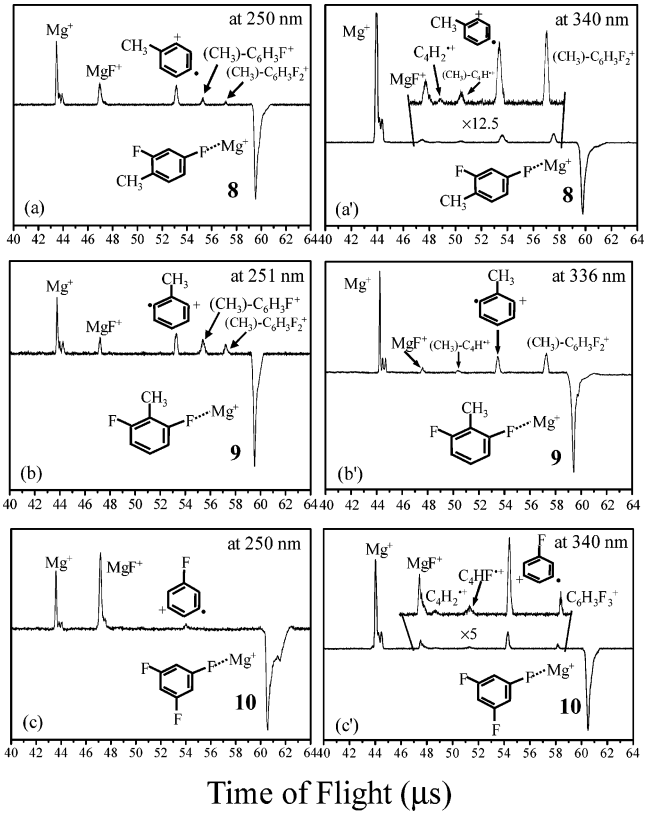

Figure 3. Photodissociation difference mass spectra of complexes with *m*-F substitutions at 250 and 340 nm.

the action spectra can be divided into Group I and Group II:

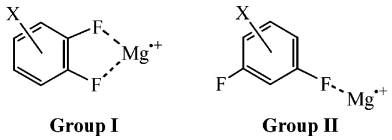

they are remarkably similar within the groups but quite different between the groups. In addition, the action spectra of the two groups are also analogous to those of $Mg^{\bullet+}$(*o*-$C_6H_4F_2$) and $Mg^{\bullet+}$-(*m*-$C_6H_4F_2$), respectively.[19] This has at least two implications. First, the two groups of complexes are distinguished by their coordination structures. In other words, Group I is featured by the coordination of $Mg^{\bullet+}$ to two neighboring F atoms, whereas Group II can only support a one-to-one coordination between $Mg^{\bullet+}$ and F. Second, the initial electronic excitation appears to be localized on the metal center $Mg^{\bullet+}$, which is relatively insensitive to the remote aromatic substituents. More specifically, the action spectra of the complexes we obtained can be assigned to the splitting of the $Mg^{\bullet+}$ $3^2P \leftarrow 3^2S$ transition under the perturbation of the F coordinations.

The splitting of the $Mg^{\bullet+}$ $3^2P \leftarrow 3^2S$ transition in the presence of substituted benzene molecules can be appreciated from a simple molecular orbital model. For all the complexes under study, the blue-shifted features in their action spectra are attributed to the promotion of the s electron of $Mg^{\bullet+}$ to the p_z orbital, which is subjected to a repulsive interaction with the lone pair electrons of the F atom or atoms. Such repulsion is more significant in monocoordinated complexes than in dicoordinated complexes because in monocoordinated complexes the p_z orbital of $Mg^{\bullet+}$ has a head-on interaction with the lone pair electron of the F atom. Consequently, this spectral peak is more blue-shifted for Group II although its position undergoes little change for the same group of complexes due to the local

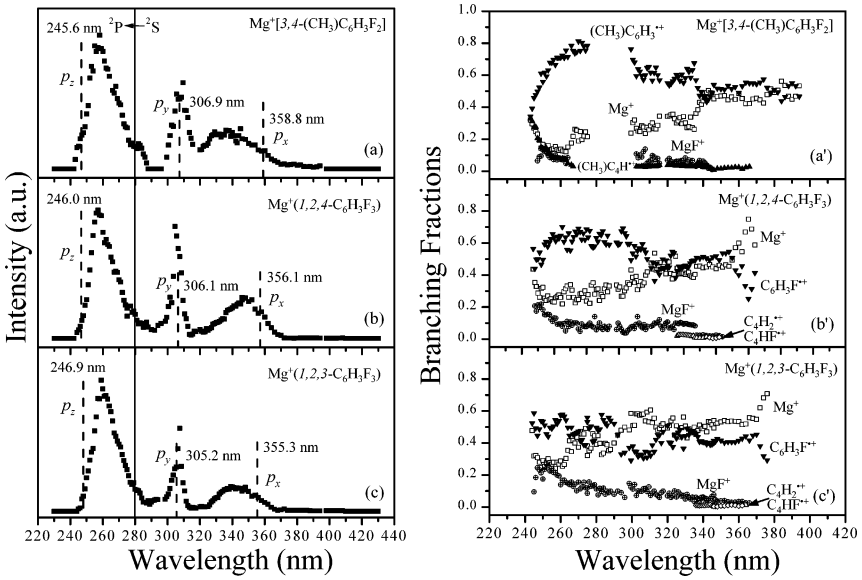

Figure 4. Action spectra and branching fraction curves of $Mg^{\bullet+}$(3,4-difluorotoluene), $Mg^{\bullet+}$(1,2,4-trifluorobenzene), and $Mg^{\bullet+}$(1,2,3-trifluorobenzene). The vertical axis represents the relative yield of all the photolysis products. The solid line indicates the atomic transition of $Mg^{\bullet+}(3^2P \leftarrow 3^2S)$ at 280 nm. The dashed lines denote the calculated absorption spectra. Note that in (a′)−(c′) only $Mg^{\bullet+}$ was observed beyond ∼380 nm, which is not shown for clarity.

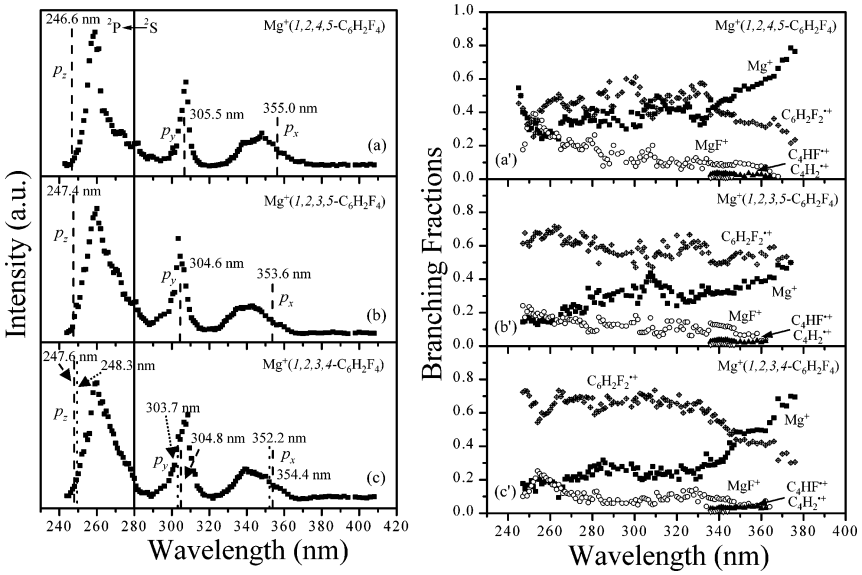

Figure 5. Action spectra and branching fraction curves of $Mg^{\bullet+}$(1,2,4,5-, 1,2,3,5-, and 1,2,3,4-tetrafluorobenzene). The vertical axis represents the relative yield of all the photolysis products. The solid line indicates the atomic transition of $Mg^{\bullet+}(3^2P \leftarrow 3^2S)$ at 280 nm. The dashed lines show the calculated absorption spectra. Note that for $Mg^{\bullet+}$(1,2,3,4-$C_6H_2F_4$) (c) the dashed lines indicate the calculated absorption spectrum for the complex with 1,2-F coordination to $Mg^{\bullet+}$, while the dotted lines are for the complex where $Mg^{\bullet+}$ is attached to the 2,3-F atoms. Note that in (a′)−(c′) only $Mg^{\bullet+}$ was observed beyond ∼380 nm, which is not shown for clarity.

nature of the excitation. Moreover, the peak appears to be sharper for Group II than for Group I (Figures 4−6). A likely explanation is that more extensive geometry rearrangement for Group I is involved upon excitation to transfer two F atoms and form the benzyne radical cations.

Clearly, the red-shifted peaks are due to the population of the p_x and p_y orbitals of $Mg^{\bullet+}$. Because p_x and p_y are nearly degenerate for Group II, the two red-shifted peaks are essentially merged for these complexes (Figure 6a,b). For Group I, the less red-shifted peak (∼305 nm) corresponds to p_y and the more red-shifted peak (355 nm) is associated with p_x on the basis of the comparison with Group II (Figures 4 and 5) and the CIS results. In other words, the interaction between the p_x orbital and the orbitals of the F atoms is analogous in the two types of complexes, whereas the p_y orbital experiences a larger repulsion in Group I than in Group II with the result of a smaller red shift from 280 to ∼305 nm. It is worth noticing that the peak at ∼305 nm corresponding to p_y is apparently sharper than other peaks. Again, this can be explained by the smaller excitation-induced geometry change of the complexes.

The two-group division of the complexes also applies to the branching curves. In general, for Group I, the branching fractions of the benzyne radical cations increase with decreasing wavelength independent of the absorption peaks. An obvious exception is the photodissociation of $Mg^{\bullet+}$(3,4-$C_7H_6F_2$), in which the branching fraction of $CH_3C_6H_3^{\bullet+}$ decreases sharply below 280 nm. This can be explained by the decomposition of the benzyne radical cation in this wavelength region. At the same time, the branching fraction of MgF^+ also increases with decreasing wavelength, indicating that the MgF^+ branching channel is

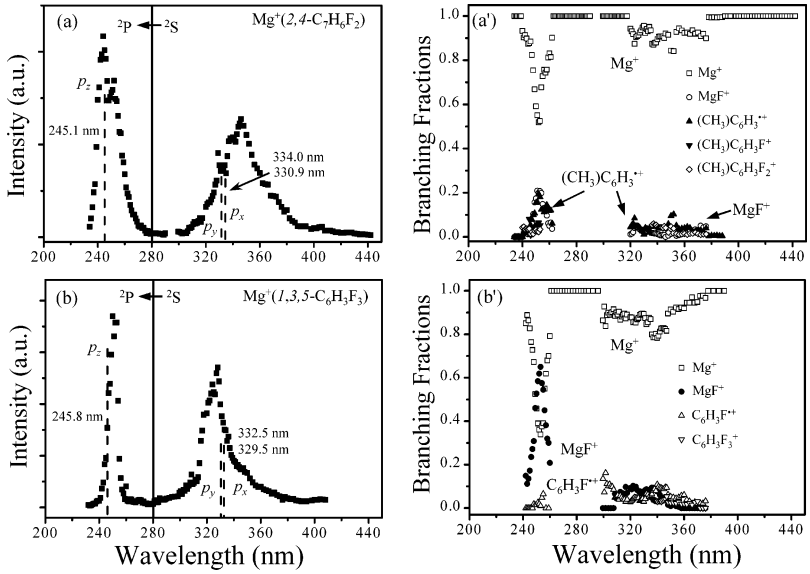

Figure 6. Action spectra (a and b) and branching fraction curves (a′ and b′) of Mg$^{\bullet+}$(2,4-difluorotoluene) and Mg$^{\bullet+}$(1,3,5-trifluorobenzene). The vertical axis represents the relative yield of all the photolysis products. The solid line indicates the atomic transition of Mg$^{\bullet+}$(3^2P←3^2S) at 280 nm. The dashed lines denote the calculated absorption spectra. For clarity, minor two-photon photoproducts are not shown in (a′) and (b′).

indeed in competition with the benzyne radical cation formation pathway (see Scheme 1). Finally, the branching fraction of Mg$^{\bullet+}$ decreases with decreasing wavelength. For Group II, the main photofragment is Mg$^{\bullet+}$, and the branching fractions of MgF$^+$ and the benzyne radical cations are small except at the absorption peaks of the complexes. This is more evident at the short wavelength absorption peak (∼250 nm). In this case, there may be at least two photodissociation pathways. The first is related to the excitation of the charge transfer state, which is relatively independent of the wavelength. The relaxation of the charge transfer states may result in a predominant production of Mg$^{\bullet+}$ and charge transfer photoproducts. The second results from the photoexcitation of Mg$^{\bullet+}$, which results in higher branching fractions of MgF$^+$ and the benzyne radical cations, although Mg$^{\bullet+}$ is also abundant. The charge transfer photoproducts of Group II (see Figure 3) are believed to be from direct dissociation because the yields are relatively insensitive to the laser wavelength (Figure 6a,b).

C. DFT Calculations. The optimized structures and relevant geometric parameters (including bond length, bond angle, atomic charge) of the complexes Mg$^{\bullet+}$[(CH$_3$)C$_6$H$_3$F$_2$], Mg$^{\bullet+}$(C$_6$H$_3$F$_3$), Mg$^{\bullet+}$(C$_6$H$_2$F$_4$), and Mg$^{\bullet+}$[(CH$_3$)C$_6$H$_2$F$_3$] (**1**−**10**) are shown in Figure 7. For the complexes (**4**, **7**, **8**) that have two possible isomers, only the stable isomers are presented. As mentioned above, Group I has a structure similar to that of Mg$^{\bullet+}$(*o*-C$_6$H$_4$F$_2$).[19] More specifically, the most stable structures of these complexes are such that Mg$^{\bullet+}$ is coordinated to two *o*-F atoms, forming a five-membered ring. The C−F bond is elongated from 1.33 to 1.39 Å by Mg$^{\bullet+}$ coordination. By comparing the methyl-substituted complexes and the fluorine-substituted complexes, we can see that the positive charge delocalization is influenced by different substituents. F is an overall electron acceptor. It reduces the positive charge delocalization from Mg$^{\bullet+}$ to the benzene ring. This leads to a weakened interaction between the Mg$^{\bullet+}$ and the two *o*-F atoms, as indicated by shorter C−F bonds and longer F−Mg bonds. On the other hand, CH$_3$ group acts as an electron donor. It promotes the positive charge delocalization from Mg$^{\bullet+}$ to the benzene ring. As a result, the complexation between Mg$^{\bullet+}$ and the two *o*-F atoms is enhanced, as demonstrated by longer C−F bonds and shorter F−Mg bonds. For Group II, the structure features are similar to that of Mg$^{\bullet+}$(*m*-C$_6$H$_4$F$_2$),[19] in which Mg$^{\bullet+}$ can only bind to one of the F atoms (see Figure 7). The C−F bond is elongated even more to 1.45 Å. Most of the positive charge remains in the Mg$^{\bullet+}$. Also, the charge separation is similar to Group I. Our calculations indicate that the bond dissociation energies (BDEs) of Group I are larger than those of Group II (see Table 1). Taking tri-F-substituted complexes (**2**, **3**, **10**) as examples, Mg$^{\bullet+}$(1,2,4-C$_6$H$_3$F$_3$) (**2**) has the largest BDE (1.16 eV), which is 0.12 eV higher than that of Mg$^{\bullet+}$(1,3,5-C$_6$H$_3$F$_3$) (**10**, BDE = 1.04 eV). Upon increasing the F substitutions, the BDEs of the complexes decrease from ∼1.4 eV (**1**, 2F and CH$_3$), to 1.1−1.2 eV (**2**−**4**, 3F or 3F and CH$_3$), to ∼1.0 eV (**5**−**7**, 4F). However, with the same number of F substitutions, the BDEs are close. For example, the tetra-F-substituted complexes share similar stabilities for a number of isomeric structures.

Besides the coordination with the F atoms, Mg$^{\bullet+}$ can also bind to the benzene π-system. Although the binding energies of such π-complexes are more sensitive to the substituents, they are all lower than the binding energies of the F−Mg$^+$ complexes (see Table 1). Therefore we believe that the complexes adopt the σ-type F−Mg$^+$ coordination. For Group II, two key intermediates (**9-I** and **10-I**) proposed for interpreting the MgF$_2$-loss process (this will be discussed later) are optimized in our calculation. The structures of **9-I** and **10-I** are presented in Figure 8. It can be seen that the F−Mg$^+$ bond lengths in **9-I** and **10-I** (1.742 and 1.738 Å) are much shorter than those in **9** and **10** (1.989 and 2.108 Å) due obviously to the stronger interaction between F and Mg$^{\bullet+}$. Surprisingly, the atomic charges of Mg$^{\bullet+}$ in **9-I** and **10-I** (+0.616 and +0.694) are much less positive than those in **9** and **10** (+0.816 and +0.848). This indicates the presence of strong interaction between FMg$^+$ and π-electrons of aromatic rings in **9-I** and **10-I**, which removes the positive charges at Mg$^{\bullet+}$. Thus, it can be expected that **9-I** and **10-I** should be very stable. Indeed, our calculation shows that the energies of **9-I** and **10-I** can be compared to those of **9** and **10** (the former two are 0.07 and 0.26 eV in energy more and less stable than the latter two, respectively). The π-complexes are crucial to the understanding of the formation of the meta-type benzyne radical cations as will be discussed in detail below.

SCHEME 1

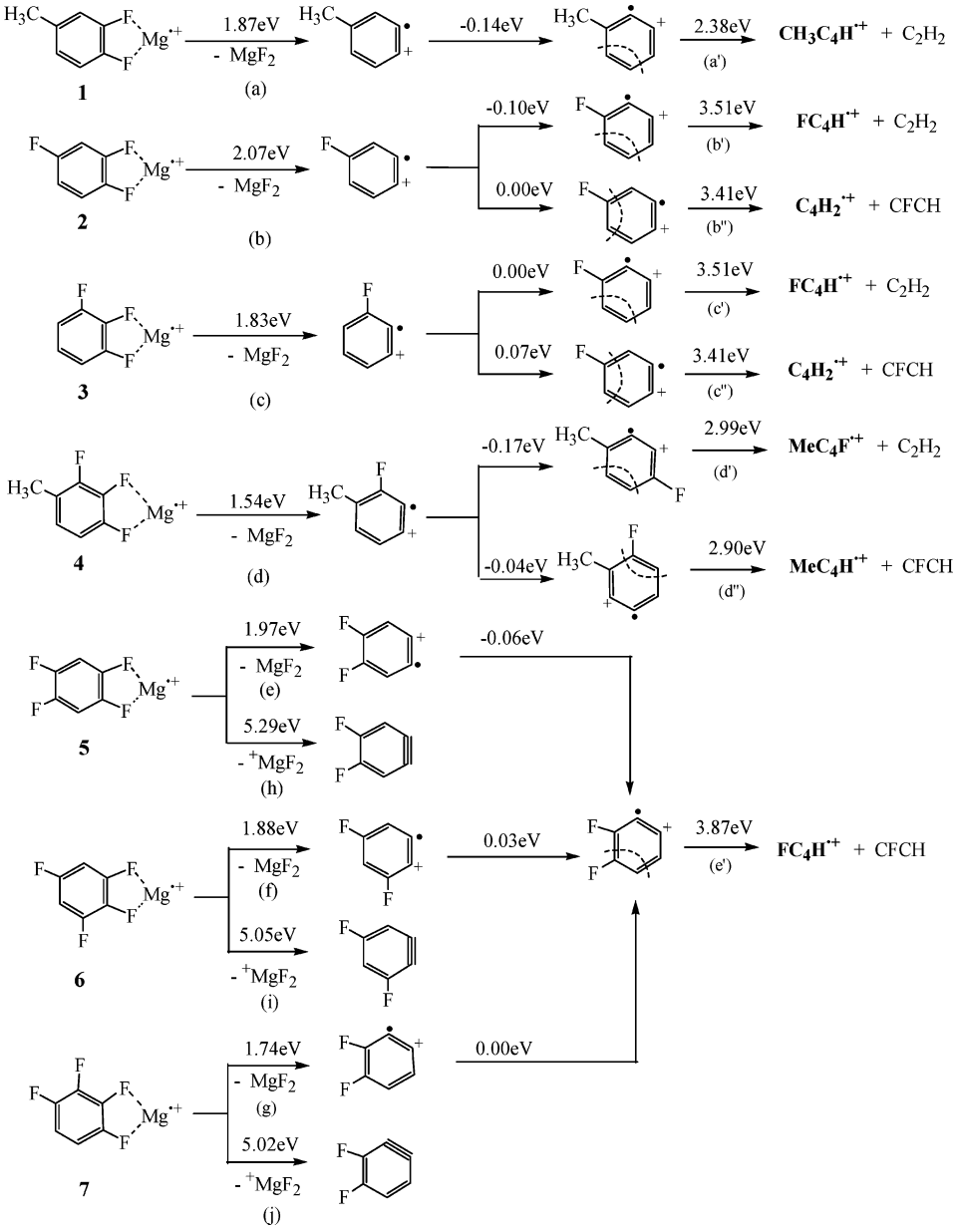

The proposed pathways for the formation and metastable decay of the benzyne radical cations are shown in Schemes 1 and 2 along with the calculated energetics. Detailed discussions on the reaction schemes will be presented in the next section.

The calculated absorption spectra of the complexes are shown in Figures 4−6 together with the action spectra for comparison. The CIS method we adopted for the calculation is a less extended configuration interaction (CI), and it was previously found to give reasonable absorption spectra.[20b] One can see here that the agreement between the action spectra and the calculated absorption spectra is remarkably good considering the crudeness of the calculation. A number of implications can be drawn here. First, the optimized structures are reasonable. Second, the photolysis is indeed started from the excitation of 3s to 3p localized on $Mg^{\bullet+}$. Third, the 3p energy level is split significantly by the presence of F-substituted benzene molecule. Finally, the reaction probabilities of the excited 3p energy sublevels appear to be similar judging from the fairly good agreement between the intensities of the action spectra and the absorption spectra. As mentioned above, the different widths of the action spectra may reflect the changes of complex structures, which will influence the ensuing nuclear dynamics.

Discussion

By aromatic substitutions, we have gained detailed information for the understanding of the photoreaction pathways for the complexes. The photoreaction patterns are classified into two groups in accordance with the coordination structure of $Mg^{\bullet+}$ to the F atoms of the fluorine-substituted benzene molecules. We have identified sequential photoreactions of the complexes including a primary reaction to form benzyne radical cations and the secondary [4 + 2] reaction. The effect of aromatic substitutions on the primary formation of the benzyne radical cations is mainly from the coordination structure of the complexes, whereas their effect on the secondary [4 + 2] decomposition of the benzyne radical cations is largely determined by the stability of the products. We will give a more detailed discussion in the following. The discussion will also be based on the two-group division of the complexes.

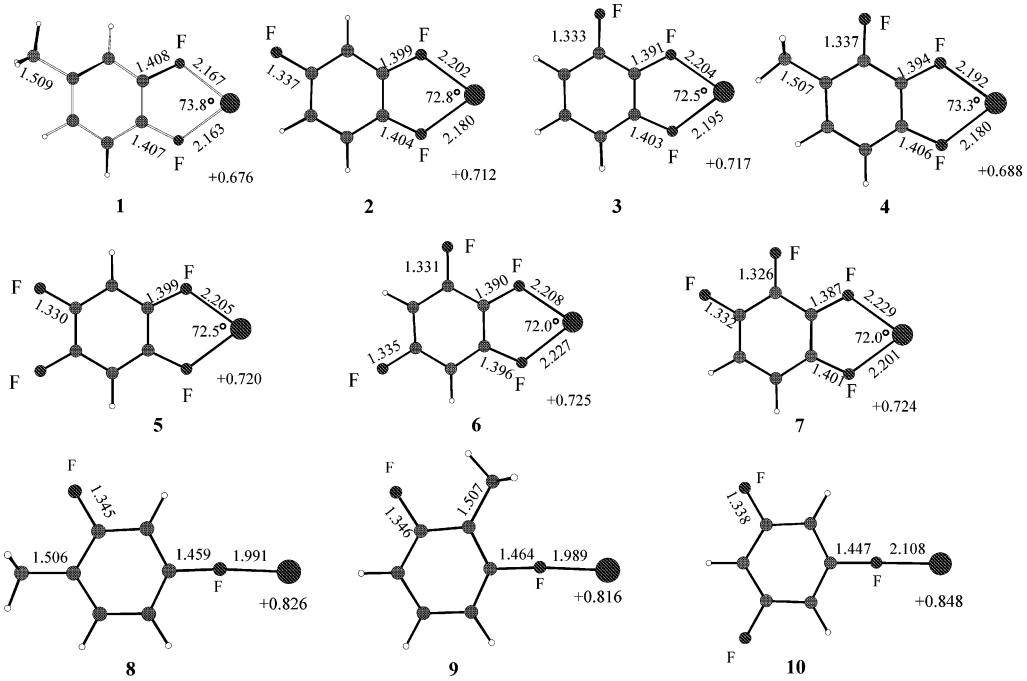

Figure 7. Optimized structures of Group I complexes (**1**−**7**) and Group II complexes (**8**−**10**). Bond lengths and angles are given in units of angstroms (Å) and degrees (°), respectively.

TABLE 1: Calculated Dissociation Energies (eV) for Complexes 1−10

	1	2	3	4	5	6	7	8	9	10
C−FMg$^+$ [a]	2.66	2.37	2.31	2.41	2.23	2.14	2.15	2.35	2.32	2.09
F−Mg$^+$ [b]	1.42	1.16	1.14	1.25	1.02	0.99	1.00	1.04	1.01	1.04
π−Mg$^+$ [c]	1.00	0.65	0.69	0.82	0.43	0.45	0.48	1.00	1.01	0.62

[a] The values of this row are the reaction energies of MgF$^{\bullet+}$ dissociation from **1**−**10**. [b] The values of this row are reaction energies of Mg$^+$ dissociation from **1**−**10**. [c] The values of this row are reaction energies of Mg$^{\bullet+}$ dissociation from π-complexes **1**−**10**.

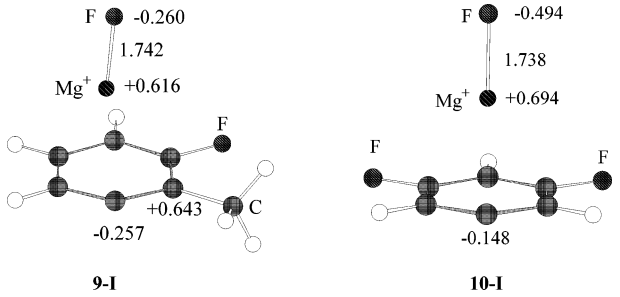

Figure 8. Optimized structures of key intermediates (**9-I** and **10-I**) for **9** and **10**, in which FMg$^+$ is π-coordinated to the aromatic ring. Bond lengths (in angstroms) and atomic charges of Mg$^{\bullet+}$ are shown.

A. Primary Photoreactions: Formation of Benzyne Radical Cations. For the photoinduced reaction patterns in Group I, the presence of a five-membered ring naturally gives rise to benzyne radical cations in ortho forms. For meta species in Group II (see Scheme 2), the formation of benzyne radical cations is more difficult in the sense that more distant F atoms have to be abstracted by Mg$^{\bullet+}$.

As depicted in Scheme 1, the ΔE values for the formation of *o*-benzyne radical cations vary from 1.54 to 2.07 eV depending on the substitutions. These energies are easily surmounted with a single ultraviolet photon used in our experiments, and therefore the *o*-benzyne radical cations were all observed with relatively high yields (see also Figures 4 and 5). Although the reaction energies are determined by the stabilities of both the complexes and the corresponding *o*-benzyne radical cations, some useful inferences can still be made. One such inference is that the formation of the benzyne radical cations bearing neighboring F atoms cost less energy. For example, the reaction energy for (c) is 0.24 eV lower than that of (b). Similar comparisons can be made for the MgF_2-loss reactions (e), (f), and (g). Two possible reasons can be considered. First, the neighboring F atoms are more effective in withdrawing the radical electrons and therefore can better stabilize the radical cations (0.08 eV between reactions b and c). Second, the neighboring F atoms are more likely to destabilize the complexes, again due to their good electron-withdrawing ability (0.16 eV between reactions b and c). Another remark is on the comparison between (a) and (b). The latter needs 0.20 eV more energy than the former due to replacement of CH_3 with the F group. We believe that the main contributing factor is the better electron-donating ability of CH_3, which serves to stabilize the *o*-benzyne radical cation. Similarly, (d) is 0.20 eV lower in energy than (g).

For the *m*-F-substituted complexes, the primary photodissociation involves either hydride transfer/scrambling to form *o*-benzynes or sequential F abstraction to form *m*-benzynes.[19] Although Br$^+$ and Cl$^+$ scrambling around the benzene ring have been reported,[23,24] the situation here with FMg$^+$ appears to be different. As shown in the bottom panel of Figure 3, although the scrambling pathway is blocked by the CH_3 group, the photoreaction pattern is still similar to those of other complexes containing *m*-F-substituted benzenes. It is likely that the successive abstraction of two F atoms involves the transient coordination of FMg$^+$ with the π-electrons of the benzenes, followed by the formation of MgF_2. This hypothesis is based on the observation of benzyne radical cation even from the complex **9** (in which two F atoms are separated by a CH_3) and also our calculated results of transition structures FMg$^+$ seated

SCHEME 2

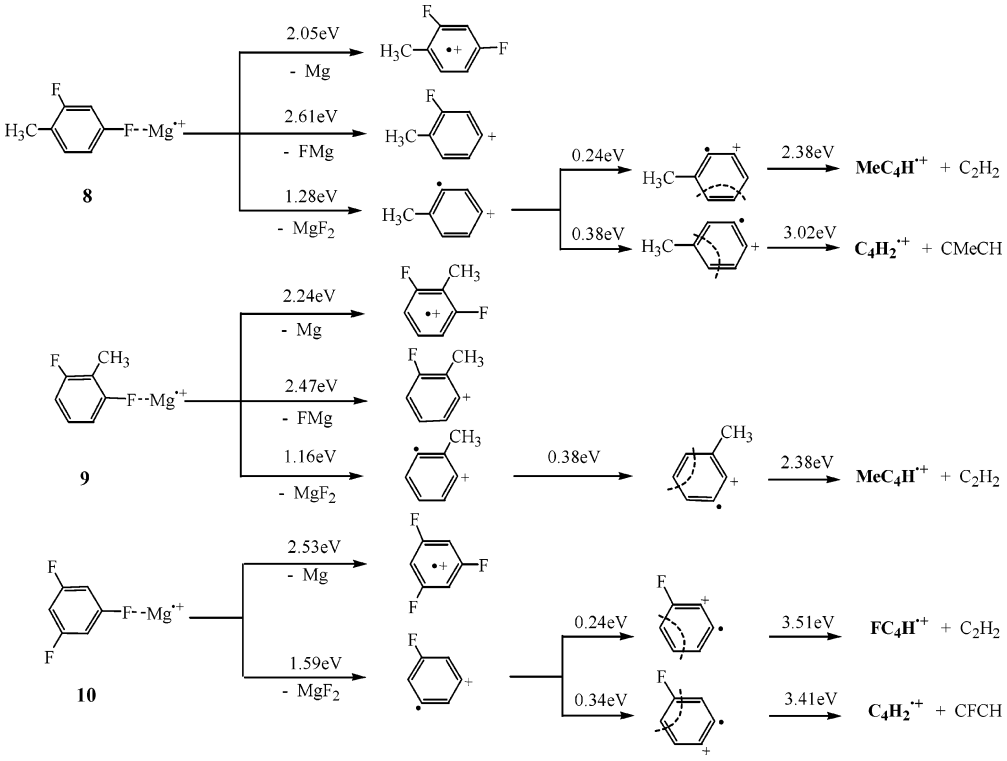

SCHEME 3

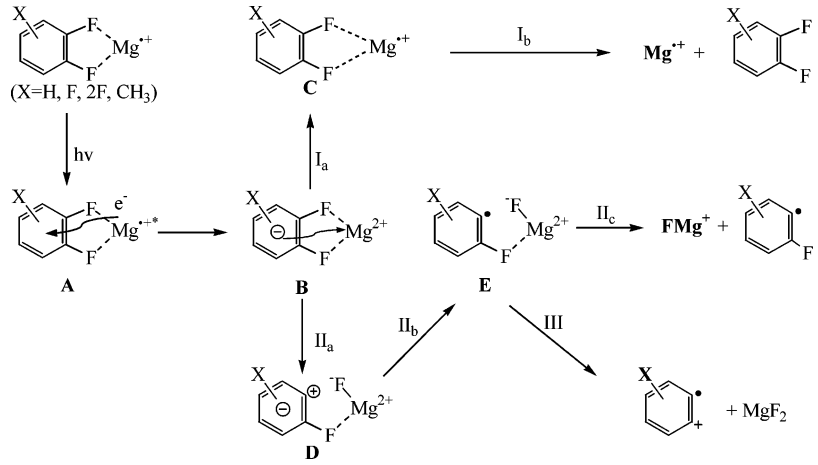

on the aromatic rings (**9-I** and **10-I**), as shown in Figure 8. According to our calculations, the ΔE for the formation of *m*-benzyne radical cations from **8**, **9**, and **10** are 1.28, 1.16, and 1.59 eV, respectively (Scheme 2). This seems to be consistent with our observation that the photoproducts **8** and **9** have higher intensities on one-photon photolysis. Because the formation mechanisms are different, we believe that the higher intensities of the *o*-benzyne radical cations are due to the lower kinetic barriers for their formation as will be discussed below.

The photolysis mechanism of Group I is similar to that of $Mg^{\bullet+}(C_6H_4F_2)$ we have studied previously.[19] After photoexcitation, $(Mg^{\bullet+})^*$ may lose the excited electron to the benzene ring, depositing most of the excitation energy to the aromatic center. Subsequently, abstraction of two F^- anions occurs perhaps in a stepwise manner, forming the stable MgF_2 molecule. A signature of the stepwise process is the detection of MgF^+, which was formed before the completion of the second F^- abstraction. For Group I, the abstraction of two F^- anions is quite efficient due to their proximity. However, this process is not as efficient for Group II, and back electron transfer from the benzene ring to Mg^{2+} may occur, exiting in the evaporation channel.

The above mechanism for the primary photolysis reactions is illustrated in Schemes 3 and 4. The electron transfer is likely to involve extensive surface crossings, which appear to direct the energy deposition to the nuclear framework of the benzene ring. The photoreaction sequence starts with the promotion of an unpaired 3s electron of $Mg^{\bullet+}$ in the complex $Mg^{\bullet+}(C_6H_{4-n}F_2X_n)$ (X = H, F, or CH_3) to an unoccupied 3p orbital, forming the intermediate **A**. This energetic electron originally on $(Mg^{\bullet+})^*$ may move to an unoccupied π-orbital of the benzene ring to form **B**. At least two relaxation pathways are possible for **B**: processes I and II. As the first possibility, the electron on the benzene ring (**B**) may jump back to Mg^{2+} (I_a), but this time it is in the 3s orbital. This creates a high vibrational excitation that tends to stretch the $Mg^{\bullet+}$−molecule linkage (**C**), and eventually evaporate the $Mg^{\bullet+}$ unit (I_b). Another possibility is that the doubly charged Mg^{2+} and the electron on the benzene

SCHEME 4

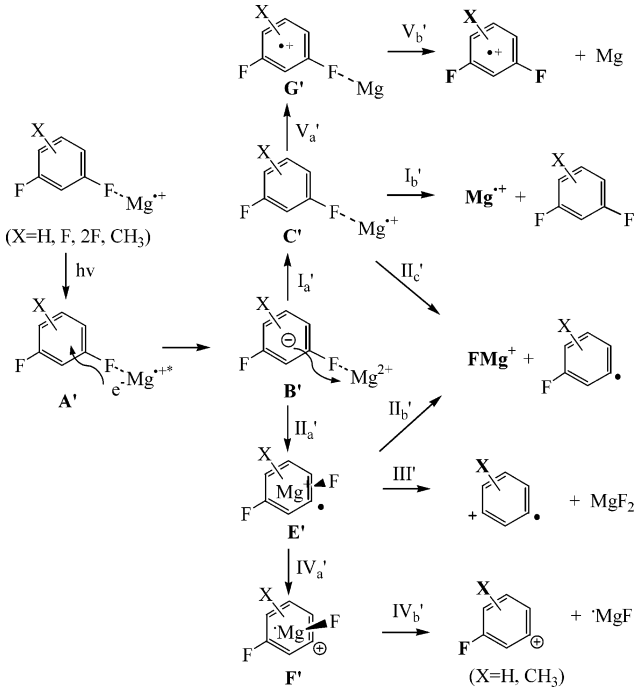

ring (**B**) may work together to activate one of the C−F bonds, leading to the heterolytic cleavage of the C−F bond (II_a) to form **D**. The transition state of the C−F bond cleavage was located, and the activation energies range from 1.00 to 1.19 eV. Such low barriers are easily overcome with the photon energies of our laser sources in both the short and long wavelength regions. The extra π-electron on the benzene ring is expected to annihilate the carbonium cation, and this makes the benzene ring highly excited. Part of **E** may end up with the formation of MgF^+ that has been observed (II_c) (for reaction energies, see Table 1 or Scheme 1). However, the high internal energy of the benzene ring and the doubly charged Mg^{2+} are more likely to cause the heterolytic breakage of the C−F bond (III), forming the benzyne radical cations as observed. A π-electron may neutralize the positive charge on the σ-orbital of the benzyne radical cation because it has been found that the π-orbital has a lower ionization energy.[7] The mechanism for the photoreactions of the *m*-F-substituted complexes appears to be similar in the first several steps, but different thereafter. The observation of $C_6H_nX_{4-n}F_2^{\bullet+}$ coupled with Mg atom is one of the differences. Such photofragments come from one more electron transfer of **C′** (V_a'), and were detected for both X = CH_3 and X = F. Unlike $C_6H_nX_{4-n}F_2^{\bullet+}$, $C_6H_nX_{4-n}F^+$ is found only in the short wavelength region for the methyl-substituted complexes presumably because the electron-donating methyl group stabilizes the benzyl cation. Another electron transfer (process IV_a') is needed to generate this side product. The failure to locate the scrambling transition state or intermediate rules out the scrambling mechanism mentioned above. An alternative possibility for the abstraction of another distant *m*-F is through the coordination of the FMg^+ group to the benzene π-system, and a stable intermediate **E′** (−0.07 to 0.26 eV relative to the parent complexes) has been successfully located (see **9-I** and **10-I** in Figure 8). Overall, Schemes 3 and 4 capture most of the features observed in our experiments for the primary photolysis reactions. In particular, the main observed products are attended to in the schemes. By refining the schemes further, all of the observed products may be accounted for.

TABLE 2: Calculated Activation Energies (eV) of Hydrogen Migration, Methyl Migration, and Fluorine Migration, and Substitutent Effect on These Activation Energies

	migration group R		
substituent X	H	CH_3	F
H	4.04	3.81	5.20
CH_3	3.85−3.92[a]		4.81−4.82[a]
F	4.33−4.46[a]	3.75−3.80[a]	5.12−5.38[a]

[a] The energy variations result from the different substitution sites of X.

It is noteworthy that the mechanism proposed in Scheme 4 can explain nicely the differences in the photodissociation of **8**−**10** (Figure 3a−c). As we know, the yield of FMg^+ from **10** is particularly high compared to those from **8** and **9** at the short wavelengths. Also, the fragment $(CH_3)C_6H_3F^+$ from **8** and **9** due to the loss of MgF is observed but the corresponding fragment $C_6H_3F_2^+$ from **10** is absent. These can be easily understood by considering the intermediates **E′** and **F′**. Because the methyl group stabilizes positive charge, the methyl-substituted intermediates **E′** and **F′** (here the former is 0.07 eV more stable than the corresponding complex) are more favorable than the fluorine-substituted intermediates (here **E′** is 0.26 eV less stable than the corresponding complex). As a result, the photoproducts from **E′** via routes II_b', III′, and IV_a' are difficult to obtain. This is consistent with our experimental observation that, for **10**, the yield of $C_6H_3F^{\bullet+}$ is relatively low and $C_6H_3F_2^{\bullet+}$ is even absent. Furthermore, because route II_a' for **10** is also unfavorable, the dissociation of **10** proceeds via route I_a' and finally gives off FMg^+ via route II_c', which explains why the branching fraction of FMg^+ is much higher at the short wavelengths (Figure 3c).

B. Metastable Decay of Benzyne Radical Cations. We have found that, given enough energy, the benzyne radical cations can all undergo further decomposition to the butadiyne radical cations and the neutral acetylene partners as highlighted with boldface type in Schemes 1 and 2. It appears that the above primary photoreaction has deposited a significant amount of energy on the benzyne radical cations, which then undergo [4 + 2] metastable decay. As described previously,[19] the [4 + 2] decomposition products increase steadily with increasing photon energy as expected for the metastable decay. This [4 + 2] ring-opening reaction is a general decomposition pathway of the benzyne radical cations we have observed for the first time. The preference of this reaction path may be related to both the energetics and the intrinsic rearrangement dynamics. It appears that *o*-benzyne radical cations are the precursors for the [4 + 2] decomposition photoproducts. For some complexes, nuclear rearrangements after the primary photoprocesses are necessary to generate the *o*-benzyne radical cation precursors for the subsequent [4 + 2] decomposition. Calculations have been carried out to evaluate the barriers for the migration on the benzyne radical cation ring. The activation energies for different migrating groups R with different substituents X are listed in Table 2.

The migrating group R is out of the benzyne plane in the transition structures (See S4-6 in Supporting Information). Therefore, the high barriers are induced due to the partial ruin of the aromatic system. Hydrogen migration and methyl migration have much lower barriers than fluorine migration. In addition, the presence of a methyl group reduces the barrier to hydrogen migration and fluorine migration by 0.1−0.3 eV. These results lead us to conclude that most of the isomerizations in Schemes 1 and 2 are accomplished by H migration instead of fluorine migration.

The high activation energies of [4 + 2] metastable decay explain that such photofragments cannot be observed in single-photon events in many complexes studied in this work. $Mg^{\bullet+}$-[3,4-$(CH_3)C_6H_3F_2$] (**1**) is an exception, and its [4 + 2] metastable decay is one photon allowed, which is consistent with the calculated lower barrier of H migration with methyl substitution.

As seen in Schemes 1 and 2, the observed products from *o*-benzyne radical cations can be accounted for in terms of the cracking patterns shown in dotted arcs. In other words, the bonds adjacent to the radical cation centers are the starting points to break presumably because of the strain induced by the neighboring radical cation centers. Upon one-photon absorption, the product $CH_3-C_4H^{\bullet+}$ from *o*-$(CH_3)C_6H_3^{\bullet+}$ was observed at both short and long wavelengths [(a′) in Scheme 1)]. It is intriguing that the other channel ($C_4H_2^{\bullet+}$ + CMeCH from *o*-$(CH_3)C_6H_3^{\bullet+}$) was not observed at all. For all the F-substituted benzyne radical cations in Scheme 1, [4 + 2] decomposition was not observed under one-photon condition. It is only after absorption of two photons that the [4 + 2] decomposition products were detected. This is quite consistent with our computation results. As shown in Scheme 1, the benzyne radical cation decomposition channel (a′) (2.38 eV) is much less endothermic than other channels. This boosts our confidence in the computational results for the systems under investigation at least in a qualitative fashion.

For substituted *m*-benzyne radical cations, as mentioned above, nuclear rearrangements are believed to occur to form *o*-benzyne radical cations before decomposition because the ring-opening decomposition patterns of *o*- and *m*-benzyne are rather similar. It should be pointed out that with the use of the energetics argument alone it is more difficult to predict the likelihood of the consecutive dissociations of the Group II complexes. For example, the consecutive dissociations of **1** are observed after absorption of one 255 nm photon, whereas they do not occur for **8** and **9** with similar energetics. Most probably, the energy deposition to the benzyne radical cations for Group II in the primary photoreactions is not as efficient as for Group I as hinted above. In the following, we will discuss separately in more detail the effects of methyl and fluorine substitutions. Before doing this, it is useful to make a further note. Implicit in the cracking patterns in Schemes 1 and 2 (dashed arcs), not only H transfer but also F and CH_3 transfer have occurred within the $C4^+$ chain in such a way that they are arranged at the edges (see Schemes 1 and 2). Although F transfer is more difficult (see Table 2), two-photon absorption provides more than sufficient energy for it to occur.

1. Methyl Substitution. In comparison to other metastable decay channels, the decomposition channel (a′) of 4-methyl-*o*-benzyne radical cation costs much less reaction energy (see Scheme 1). This explains why only the cation $CH_3-C_4H^{\bullet+}$ but not $C_4H_2^{\bullet+}$ was observed after one-photon absorption (see Figures 1 and 4). It is understandable that the electron-donating CH_3 group can stabilize the butadiyne radical cation, resulting in the more facile process (a′).

For the decomposition of methyl-substituted *m*-benzyne radical cation, $CH_3-C_4H^{\bullet+}$ was still dominant although $C_4H_2^{\bullet+}$ was also observed. It should be pointed out that the products were observed only after two-photon absorption, in sharp contrast to the case of methyl-substituted *o*-benzyne radical cations. This is clearly associated with the structural difference of *m*-$(CH_3)C_6H_3^{\bullet+}$ and *o*-$(CH_3)C_6H_3^{\bullet+}$. A plausible explanation is that the meta-type benzyne radical cation is more stable than the ortho-type benzyne radical cation and its conversion to the ortho type is energetically unfavorable. In addition, much of the received photon energy may have been lost in the primary photoprocess because two farther F atoms have to be abstracted for the meta-type benzyne radical cation.

2. Fluorine Substitution. We found that the [4 + 2] decomposition of all-fluorine-substituted benzyne radical cations is possible only with two photons (Figures 1−3). This is supported by the calculations (Schemes 1 and 2), which predict much higher energies for the decomposition of the all-fluorine-substituted benzyne radical cations than that of the methyl-substituted benzyne radical cation. F is a strong σ-electron acceptor, which destabilizes both the reactants (benzyne radical cations) and products. However, F appears to destabilize the products to a much larger extent because it displays a strong σ-electron-withdrawing character, whereas it may be a π-electron donor in the carbon π-system such as the benzyne radical cations. For example, the energies for the decomposition pathways (b′) (3.51 eV) and (b″) (3.41 eV) of mono-F-substituted benzyne radical cations are substantially larger than that of (a′). Because the stability difference between the two monofluorine-substituted *o*-benzyne radical cations is only ~0.07 eV, the decomposition energies are mainly determined by the stability of the [4 + 2] decomposition products. The fact that both $C_4H_2^{\bullet+}$ and $C_4HF^{\bullet+}$ were observed after two-photon absorption is consistent with the comparable energies of (b′) and (b″) and those of (c′) and (c″) obtained from our calculations.

The difluorine substitution has an even more significant effect on the decomposition energies of the *o*-benzyne radical cations (3.87 eV), owing again to the destabilization of the [4 + 2] decomposition products. There are three possible [4 + 2] decomposition pathways for difluorine-substituted *o*-benzyne radical cations: (1) $C_4H_2^{\bullet+}$ + CF≡CF (ΔE = 4.08 eV); (2) $C_4HF^{\bullet+}$ + CF≡CH (ΔE = 3.87 eV); (3) $C_4F_2^{\bullet+}$ + CH≡CH (ΔE = 4.08 eV). In our experiments, only pathway 2 was observed with a two-photon excitation (Figure 2). Obviously, the low decomposition energy is partially the reason here. However, perhaps more important is the dynamics that determines the cracking patterns. As mentioned above, the cracking is generally adjacent to the benzyne radical cation centers (see the dashed arcs in Scheme 1). Although F transfer may occur after cracking within the $C4^+$ unit, it is expected to be difficult before cracking. Consequently, such cracking patterns can only yield products corresponding to pathway 2 as observed. For *m*-$C_6H_3F^{\bullet+}$, two $C4^+$ photoproducts $C_4HF^{\bullet+}$ and $C_4H_2^{\bullet+}$ were also detected when the parent complex absorbed more than one photon, which is similar to that found for *o*-$C_6H_3F^{\bullet+}$ (Figure 1b′,c′).

Conclusion

We have performed a comprehensive study on the remarkable photoinduced reactions in the complexes of $Mg^{\bullet+}$ and methyl- and fluoro-substituted benzene molecules. Two groups of complexes have been examined (Group I and Group II), which are distinguished by their structural/spectroscopic features, photolysis pathways, and branching ratios. The complexes of Group I involve ortho substitutions of F atoms that are bidentate coordinated to $Mg^{\bullet+}$, whereas those of Group II feature the linkage of $Mg^{\bullet+}$ to only one of the F atoms. Photolysis of the Group I complexes produced predominantly the *o*-benzyne radical cations, whereas that of the Group II complexes yielded the benzyne radical cations much less efficiently. For each group of complexes, different substituents, including CH_3 (medium σ-electron donor) and F (strong σ-electron acceptor and weak π-electron donor) affect the branching ratios significantly; i.e., they result in different decomposition thresholds of the *o*-

benzyne radical cations. Through the substitution studies, we have identified photolysis pathways of the complexes. With the help of quantum mechanics calculations, the observed substitutent effects on the photoformation and decompositions of the substituted *o*-benzyne radical cations are explained primarily from the energy point of view. Possible [4 + 2] decomposition mechanisms of the substituted *o*-benzyne radical cation rings are discussed. We have also proposed a reasonable mechanism for the formation of *m*-benzyne radical cations, which involves a π-$^{+}$MgF intermediate. The rich photoreaction dynamics of the complexes may be probed further by femtosecond pump−probe experiments. These complexes appear to be a good model system for the understanding of electron transfer and atomic rearrangement in chemical reactions.

Acknowledgment. This work was supported by an RGC grant administered by the UGC of Hong Kong.

Supporting Information Available: Geometries, Cartesian coordinates, and energetics of parent complexes, benzyne radical cations, and transition structures. This material is available free of charge via the Internet at http://pubs.acs.org.

References and Notes

(1) Wenk, H. H.; Winkler, M.; Sander, W. *Angew. Chem., Int. Ed.* **2003**, *43*, 502, and references therein.

(2) (a) Jones, R. R.; Bergmann, R. G. *J. Am. Chem. Soc.* **1972**, *94*, 660. (b) Bergmann, R. G. *Acc. Chem. Res.* **1973**, *6*, 25. (c) Bharucha, K. N.; Marsh, R. M.; Minto, R. E.; Bergaman, R. G. *J. Am. Chem. Soc.* **1992**, *114*, 3120.

(3) (a) Pratviel, G.; Bernadon, J.; Meunier, B. *Angew. Chem., Int. Ed. Engl.* **1995**, *34*, 746. (b) Kraka, E.; Cremer, D. *J. Am. Chem. Soc.* **2000**, *122*, 8245.

(4) Nicolaou, K. C.; Dai, W.-M. *Angew. Chem., Int. Ed. Engl.* **1991**, *103*, 1453. (b) Nicolaou, K. C.; Smith, J. A. *Acc. Chem. Res.* **1992**, *25*, 497. (c) Paloma, L. G.; Smith, J. A.; Chazin, W. J.; Nicolaou, K, C. *J. Am. Chem. Soc.* **1994**, *116*, 3697.

(5) (a) Sander, W. *Acc. Chem. Res.* **1999**, *32*, 669. (b) Wenk, H. H.; Sander, W. *Eur. J. Org. Chem.* **1992**, *57*, 7. (c) Sander, W.; Exner, M. *J. Chem. Soc., Perkin Trans. 2* **1999**, 2285. (d) Wenk, H. H.; Sander, W. *Chem. Eur. J.* **2001**, *7*, 1837. (e) Wenk, H. H.; Balster, A.; Sander, W. Hrovat, D. A.; Borden, W. T. *Angew. Chem., Int. Ed.* **2002**, *40*, 2295.

(6) (a) Radziszewski, J. G.; Waluk, J.; Kaszynski, P.; Spanget-Larsen, J. *J. Phys. Chem. A* **2002**, *106*, 6730. (b) Johnson, W. T.; Cramer, C. J. *J. Am. Chem. Soc.* **2001**, *123*, 923.

(7) Zhang, X.; Chen, P. *J. Am. Chem. Soc.* **1992**, *114*, 3147.

(8) Diau, E. W.-G.; Casanova, J.; Roberts, J. D.; Zewail, A. H. *Proc. Natl. Acad. Sci. U.S.A.* **2000**, *97*, 1376.

(9) (a) Kraka, E.; Cremer, D. *Chem. Phys. Lett.* **1993**, *216*, 333. (b) Kraka, E.; Cremer, D.; Bucher, G.; Sander, W. *Chem. Phys. Lett.* **1997**, *268*, 313. (c) Grafenstein, J.; Hjerpe, A. M.; Kraka, E.; Cremer, D. *J. Phys. Chem. A* **2000**, *104*, 1748. (d) Winkler, M.; Sander, W. *J. Phys. Chem. A* **2001**, *105*, 10422. (e) Kraka, E.; Anglada, J.; Hjerpe, A.; Filatov, Cremer, D. *Chem. Phys. Lett.* **2001**, *348*, 115. (f) Kraka, E.; Cremer, D. J. *J. Am. Chem. Soc.* **2000**, *122*, 8245.

(10) Clark, A. E.; Davison, E. R. *J. Am. Chem. Soc.* **2001**, *123*, 10691.

(11) (a) Schottelius, M.; Chen, P. *J. Am. Chem. Soc.* **1996**, *118*, 4896. (b) Logan, C. F.; Chen, P. *J. Am. Chem. Soc.* **1996**, *118*, 2113.

(12) (a) Wenthold, P. G.; Squires, R. R. *J. Am. Chem. Soc.* **1994**, *116*, 6961. (b) Wenthold, P. G.; Hu, J.; Squires, R. R. *J. Am. Chem. Soc.* **1996**, *118*, 11865. (c) Wenthold, P. G.; Squires, R. R.; Linberger, W. C. *J. Am. Chem. Soc.* **1998**, *120*, 5279. (d) Wenthold, P. G.; Hu, J.; Squires, R. R. *J. Mass Spectrom.* **1998**, *33*, 796. (e) Nash, J. J.; Squires, R. R. *J. Am. Chem. Soc.* **1996**, *118*, 11872.

(13) Guo, Y. L.; Grabowski, J. J. *J. Am. Chem. Soc.* **1991**, *113*, 5923.

(14) (a) Xu, Y. C.; Chen, Q.; Poehlein, S. K.; Freiser, B. S. *Rapid Commun. Mass Spectrom.* **1999**, *13*, 645. (b) Huang, Y.; Freiser, B. S. *J. Am. Chem. Soc.* **1989**, *111*, 2387. (c) Huang, Y.; Freiser, B. S. *J. Am. Chem. Soc.* **1990**, *112*, 1682. (d) Garcia, E.; Huang, Y.; Freiser, B. S. *Inorg. Chem.* **1993**, *32*, 3595. (e) Xu, Y. C.; Lee, S. A.; Freiser, B. S. *J. Am. Chem. Soc.* **1995**, *117*, 5413.

(15) Gibson, J. K. *J. Phys. Chem.* **1996**, *100*, 15688.

(16) Moini, M.; Leroi, G. E. *J. Phys. Chem.* **1986**, *90*, 4002.

(17) Muntean, F.; Heumann, L.; Armentrout, P. B. *J. Chem. Phys.* **2002**, *116*, 5593.

(18) Rosenstock, H. M.; Dannacher, J.; Liebman, J. F. *Radiat. Phys. Chem.* **1982**, *40*, 7.

(19) Liu, H. C.; Wang, C. S.; Guo, W. Y.; Wu, Y.-D.; Yang, S. H. *J. Am. Chem. Soc.* **2002**, *124*, 3794.

(20) (a) Yang, X.; Hu, Y. H.; Yang, S. H. *J. Phys. Chem. A* **2000**, *104*, 8496. (b) Yang, X.; Liu, H. C.; Yang, S. H. *J. Chem. Phys.* **2000**, *113*, 3111. (c) Yang, X.; Gao, K. L.; Liu, H. C.; Yang, S. H. *J. Chem. Phys.* **2000**, *112*, 10236.

(21) Frisch, M. J.; Trucks, G. W.; Schlegel, H. B.; Scuseria, G. E.; Robb, M. A.; Cheeseman, J. R.; Zakrzewski, V. G.; Montgomery, J. A., Jr,; Stratmann, R. E.; Burant, J. C.; Dapprich, S.; Millam, J. M.; Daniels, A. D.; Kudin, K. N.; Strain, M. C.; Farkas, O.; Tomasi, J.; Barone, V.; Cossi, M.; Cammi, R.; Mennucci, B.; Pomelli, C.; Adamo, C.; Clifford, S.; Ochterski, J.; Petersson, G. A.; Ayala, P. Y.; Cui, Q.; Morokuma, K.; Malick, D. K.; Rabuck, A. D.; Raghavachari, K.; Foresman, J. B.; Cioslowski, J.; Ortiz, J. V.; Baboul, A. G.; Stefanov, B. B.; Liu, G.; Liashenko, A.; Piskorz, P.; Komaromi, I.; Gomperts, R.; Martin, R. L.; Fox, D. J.; Keith, T.; Al-Laham, M. A.; Peng, C. Y.; Nanayakkara, A.; Gonzalez, C.; Challacombe, M.; Gill, P. M. W.; Johnson, B. G.; Chen, W.; Wong, M. W.; Andres, J. L.; Gonzalez, C.; Head-Gordon, M.; Replogle, E. S.; Pople, J. A. *Gaussian 98*, Revision A.7; Gaussian, Inc.: Pittsburgh, PA, 1998.

(22) (a) Bally, T.; Sastry, G. N. *J. Phys. Chem. A* **1997**, *101*, 7923. (b) Crawford, T. D.; Kraka, E.; Stanton, J. F.; Cremer, D. *J. Chem. Phys.* **2001**, *114*, 10638. (c) Braida, B.; Lauvergnat, D.; Hiberty, P. C. *J. Chem. Phys.* **2001**, *115*, 90. (d) Koga, N.; Morokuma, K. *J. Am. Chem. Soc.* **1991**, *113*, 1907. (e) Galbraith, J. M.; Schreiner, P. R.; Harris, N.; Wei, W.; Wittkopp, A.; Shaik, S. *Chem. Eur. J.* **2000**, *6*, 1446. (f) Grafenstein, J.; Hjerpe, A. M.; Kraka, E.; Cremer, D. *J. Phys. Chem. A* **2000**, *104*, 1748. (g) Kraka, E.; Anglada, J.; Hjerpe, A.; Filatov, M.; Cremer, D. *Chem. Phys. Lett.* **2001**, *348*, 115.

(23) Moini, M.; Leroi, G. E. *J. Phys. Chem.* **1986**, *90*, 4002.

(24) Friedman, R. S.; Andrews, L. *J. Am. Chem. Soc.* **1985**, *107*, 822.